VIII International Conference on Computational Methods for Coupled Problems in Science and Engineering
COUPLED PROBLEMS 2019
E. Oñate, M. Papadrakakis and B. Schrefler (Eds)

THERMO-MECHANICAL COUPLING IN FIBER-REINFORCED CONTINUA: MIXED FINITE ELEMENT FORMULATIONS AND ENERGY-MOMENTUM TIME INTEGRATION

Dietzsch J.*, Groß M.† and Flessing L.††

Technische Universität Chemnitz
Professorship of applied mechanics and dynamics
Reichenhainer Straße 70, D-09126 Chemnitz

* julian.dietzsch@mb.tu-chemnitz.de † michael.gross@mb.tu-chemnitz.de

†† tmd@mb.tu-chemnitz.de

Key words: Mixed finite element method, higher-order energy-monentum scheme, fiber-reinforced material, polyconvex strain energy function, anisotropic thermoelasticity

Abstract. Our research activity is motivated by accurate dynamic simulations of fiber-reinforced materials in light-weight structures. In order to accomplish this, we have to take various steps. The material behavior is formulated with an anisotropic, polyconvex strain energy function. We combine different mixed element formulations (e.g. see Reference [2] or [3]) with a Galerkin time integrator as shown in Reference [5]. This reduces the volumetric locking effect of an incompressible matrix material as well as the locking effect due to stiff fibers. In addition, we increase the accuracy by using Galerkin-based higher-order time integrators. Since in long-term simulations a hugh energy error is a strong problem, we apply the mixed finite element formulations to an energy-momentum time integration scheme (see Reference [6]). In the next step, we extend the material formulation by adding a thermo-mechanical coupling as shown in Reference [7]. Here we also describe the directional heat conduction of the fiber. As numerical examples with multiple material domains and families of fibers serve cooks cantilever beam as in Reference [5]. The Dirichlet boundary conditions are modelled by the Lagrange-multiplier method (see Reference [7]) and as Neumann boundary condition a pressure distribution is used.

1 INTRODUCTION

The accurate dynamic simulation of fiber-reinforced materials in light-weight structures plays an increasing role. Meanwhile these materials are used in many areas such as

aircrafts, automobiles and wind power plants. In addition to the low density and the high modulus of elasticity, the thermal properties also play a crucial role. For example the low thermal expansion of the matrix part, as well as the possibility to conduct the heat directionally with the fibers. Therefore, in this paper, we present the dynamic behavior of a thermoelastic anisotropic continuum, where the different fibers and the matrix part have different thermal parameters.

By using the mentioned materials, we have on the one hand volumetric locking effects of an incompressible matrix material and on the other hand, locking effects due to stiff fibers. A first formulation that prevents volumetric locking successfully is described in Reference [1]. Here, the volumetric dilatation is approximated independently from the deformation gradient. Futhermore, this formulation was improved again in Reference [2] by approximating the cofactor also as an independent field. A possibility to overcome the locking of the fiber is shown in Reference [3]. Here an independent approximation of the right Cauchy-Green tensor for the anisotropic part of the strain energy function is done. In Reference [5] this method is reformulated in the fourth invariant and another field for the fifth invariant is introduced. In addition, the invariant method can also be represented in tensors, but the results for both methods are the same (see Reference [5]). The tensor variant has the advantage to use several fibers without further implementation effort for the element formulation.

In order to perform exact dynamic simulations and therefore to enable long-term simulations, it is necessary to provide higher-order time integrators. Thereby Galerkin-based higher-order time integrators are a good option. In addition, a hugh energy error is a strong problem and so we have to apply energy-momentum time integration schemes (see Reference [6]).

It is only logical to combine these methods and thus to combine the advantages of these methods. On the basis of Reference [7], we combine the Hu-Washizu functionals shown in Reference [5] with the mixed principle of virtual power and thus obtain a thermo-mechanical formulation for the various mixed elements and a Galerkin-based higher-order time integrators. Here, the Dirichlet boundary conditions are modelled by the Lagrange-multiplier method and a Neumann boundary condition in the form of a pressure distribution will also be provided. In addition, we extend the continuum in such a way, that we can model different families of fibers and directional heat conduction of the fibers.

In the current paper, we first define the continum model and the finite element formulation. Then, with the help of the mixed principle of virtual power, we obtain the weak forms. Finally, we make various numerical studies on cook's cantilever beam. Here we can show the excellent convergence behaviour of the mixed elements and the positive effect on the computational time. In addition, the advantages of using different fibres in the same continuum can be demonstrated, as their different properties can be used more purposefully.

2 CONTINUUM MODEL

As continuum model, we consider an anisotropic material with n_F fiber directions $\mathbf{a}_0^i$ moving in the Euclidean space $\mathbb{R}^{n_{\text{dim}}}$ with the constant ambient temperature Θ_∞. With the structural tensor $\boldsymbol{M}_i = \boldsymbol{a}_0^i \otimes \boldsymbol{a}_0^i$, the right Cauchy-Green tensor $\boldsymbol{C} = \boldsymbol{F}^T\boldsymbol{F}$ and the absolute temperature Θ, we define the strain energy function, which is split into a single matrix part Ψ_M and multiple fiber parts Ψ_{F_i}, given by

$$\Psi(\boldsymbol{C}, \Theta, \boldsymbol{M}) = \Psi_M(\boldsymbol{C}, \Theta) + \sum_{i=1}^{n_F} \Psi_{F_i}(\boldsymbol{C}, \Theta, \boldsymbol{M}_i) \tag{1}$$

By taking into account $J = \det[\boldsymbol{F}] = \sqrt{\det[\boldsymbol{C}]}$, we assume the specific dependencies

$$\Psi_M(\boldsymbol{C}, \operatorname{cof}[\boldsymbol{C}], J, \Theta) = \Psi_M^{iso}(\boldsymbol{C}, \operatorname{cof}[\boldsymbol{C}], J) + \Psi_M^{vol}(J) + \Psi_M^{cap}(\Theta) + \Psi_M^{coup}(\Theta, J) \tag{2}$$

$$\Psi_{F_i}(\boldsymbol{C}, \operatorname{cof}[\boldsymbol{C}], J, \Theta, \boldsymbol{M}_i) = \Psi_{F_i}^{ela}(\boldsymbol{C}, \operatorname{cof}[\boldsymbol{C}], J, \boldsymbol{M}_i) + \Psi_{F_i}^{cap}(\Theta) + \Psi_{F_i}^{coup}(\Theta, \boldsymbol{C}, \boldsymbol{M}_i) \tag{3}$$

The elastic part of the matrix part Ψ_M is split into an isochoric part Ψ_M^{iso} and a volumetric part Ψ_M^{vol}. The thermo-elastic free energy of the matrix is subdivided into a heat capacity part Ψ_M^{cap}, and the part of the thermo-mechanical coupling effect, which takes the form

$$\Psi_M^{coup}(\Theta, J) = -2n_{\text{dim}}\beta_M(\Theta - \Theta_\infty)J\frac{\partial\Psi_M^{vol}(J)}{\partial J}, \tag{4}$$

where β_M ist the coefficient of linear thermal expansion for the matrix part. For the fibres, the thermal part is separated in the same way. We assume heat capacity parts $\Psi_{F_i}^{cap}$ as well as parts of the thermo-mechanical coupling

$$\Psi_{F_i}^{coup}(\Theta, \boldsymbol{C}, \boldsymbol{M}_i) = -2\beta_{F_i}(\Theta - \Theta_\infty)\sqrt{I_4^i}\frac{\partial\Psi_{F_i}^{ela}(I_4^i, \dots)}{\partial I_4^i}, \tag{5}$$

with the fourth invariant $I_4^i(\boldsymbol{C}, \boldsymbol{M}_i) = \operatorname{tr}[\boldsymbol{C}\boldsymbol{M}_i]$ and the coefficients of linear thermal expansion for the fiber parts β_{F_i}.

3 FINITE ELEMENT FORMULATION

For the formulation of finite element discretizations in space, we use Hu-Washizu functionals Π_{HW}. With the assumed temperature field $\tilde{\Theta}$ and the entropy density field η as the corresponding Lagrange multiplier, the complete functional of the internal energy is

$$\Pi^{\text{int}} = \Pi_{HW} + \int_{\mathcal{B}_0} \eta\ (\Theta - \tilde{\Theta})\mathrm{d}V \tag{6}$$

The functional of the standard displacement element reads

$$\Pi_{HW}^D(\boldsymbol{q}, \Theta) = \int_{\mathcal{B}_0} \Psi(\boldsymbol{C}(\boldsymbol{q}), \Theta, \boldsymbol{M})\mathrm{d}V \tag{7}$$

Table 1: Prescribed simulation parameters for Cook's cantilever beam.

$\epsilon_1 = 0.1e6$	$\epsilon_6 = 10e6$	$k_M = 0.1$	$k_{F_1} = 0.1$	$k_{F_2} = 50$
$\epsilon_2 = 0.1e6$	$\epsilon_7 = 4$	$\beta_M = 1e-7$	$\beta_{F_1} = 1e-9$	$\beta_{F_2} = 1e-10$
$\epsilon_3 = 1.8e6$	$\epsilon_8 = 4$	$c_M^0 = 1500$	$c_{F_1}^0 = 1500$	$c_{F_2}^0 = 3000$
$\epsilon_4 = 100e6$	$\epsilon_9 = 1$	$c_M^1 = 0.003$	$c_{F_1}^1 = 0.003$	$c_{F_2}^1 = 0.006$
$\epsilon_5 = 4$	$\epsilon_{10} = 0.1e6$	$\rho_0 = 1000$	$\Theta_\infty = 300$	
$h_n = 0.005$	$T = 1.0$	$TOL = 1e-4$	$\hat{p} = 1.5e6$	

Table 2: Numbering of the polynomial degrees.

digit nr.:	1	2	3	4	5	6
pol. degree of:	$\boldsymbol{q}$,Θ	$\boldsymbol{H}$,$\boldsymbol{B}$	$\tilde{J}$,$\tilde{p}$	$\boldsymbol{C}_A$,$\boldsymbol{S}_A$	$\boldsymbol{H}_A$,$\boldsymbol{B}_A$	$\tilde{J}_A$,$\tilde{p}_A$

With the introduction of an independent variable for the volumetric dilatation $\tilde{J}$, we obtain the displacement-pressure element introduced by Simo et al. in [1]. Here, the corresponding Lagrange multiplier $\tilde{p}$ plays the role of the hydrostatic pressure. The corresponding functional takes the form

$$\Pi_{HW}^{DP}(\boldsymbol{q}, \Theta, \tilde{J}, \tilde{p}) = \Pi_{HW}^{D} + \int_{\mathcal{B}_0} \tilde{p}\ (J(\boldsymbol{q}) - \tilde{J})\mathrm{d}V \quad \text{with} \tag{8}$$

$$\Psi_M(\dots) = \Psi_M^{iso}(\boldsymbol{C}, \mathrm{cof}[\boldsymbol{C}], \tilde{J}) + \Psi_M^{vol}(\tilde{J}) + \Psi_M^{cap}(\Theta) + \Psi_M^{coup}(\Theta, \tilde{J}) \tag{9}$$

$$\Psi_{F_i}(\dots) = \Psi_{F_i}^{ela}(\boldsymbol{C}, \mathrm{cof}[\boldsymbol{C}], \tilde{J}, \boldsymbol{M}_i) + \Psi_{F_i}^{cap}(\Theta) + \Psi_{F_i}^{coup}(\Theta, \boldsymbol{C}, \boldsymbol{M}_i) \tag{10}$$

A third functional is shown in Reference [2]. Here an additional field for the cofactor of $\boldsymbol{C}$ is introduced, such that we arrive at the functional

$$\Pi_{HW}^{CoFEM}(\boldsymbol{q}, \Theta, \dots, \boldsymbol{H}, \boldsymbol{B}) = \Pi_{HW}^{DP} + \int_{\mathcal{B}_0} \boldsymbol{B} : (\mathrm{cof}[\boldsymbol{C}(\boldsymbol{q})] - \boldsymbol{H})\mathrm{d}V \quad \text{with} \tag{11}$$

$$\Psi_M(\dots) = \Psi_M^{iso}(\boldsymbol{C}, \boldsymbol{H}, \tilde{J}) + \Psi_M^{vol}(\tilde{J}) + \Psi_M^{cap}(\Theta) + \Psi_M^{coup}(\Theta, \tilde{J}) \tag{12}$$

$$\Psi_{F_i}(\dots) = \Psi_{F_i}^{ela}(\boldsymbol{C}, \boldsymbol{H}, \tilde{J}, \boldsymbol{M}_i) + \Psi_{F_i}^{cap}(\Theta) + \Psi_{F_i}^{coup}(\Theta, \boldsymbol{C}, \boldsymbol{M}_i) \tag{13}$$

Especially for anisotropic material formulations another element (called SKA element) is presented in Reference [3]. This introduces an additional field $\boldsymbol{C}_A$ for the anisotropic part Ψ^{ani} of the material formulation. The anisotropic part of the stress tensor is represented by the corresponding Lagrange multiplier $\boldsymbol{S}_A$. Here, we arrive at

$$\Pi_{HW}^{CoSKA}(\boldsymbol{q}, \Theta, \dots, \boldsymbol{C}_A, \boldsymbol{S}_A) = \Pi_{HW}^{CoFEM} + \int_{\mathcal{B}_0} \frac{1}{2}\boldsymbol{S}_A : (\boldsymbol{C} - \boldsymbol{C}_A)\mathrm{d}V \quad \text{with} \tag{14}$$

$$\Psi_M(\dots) = \Psi_M^{iso}(\boldsymbol{C}, \mathrm{cof}[\boldsymbol{C}], \tilde{J}) + \Psi_M^{vol}(\tilde{J}) + \Psi_M^{cap}(\Theta) + \Psi_M^{coup}(\Theta, \tilde{J}) \tag{15}$$

$$\Psi_{F_i}(\dots) = \Psi_{F_i}^{ela}(\boldsymbol{C}_A, \mathrm{cof}[\boldsymbol{C}_A], \sqrt{\det[\boldsymbol{C}_A]}, \boldsymbol{M}_i) + \Psi_{F_i}^{cap}(\Theta) + \Psi_{F_i}^{coup}(\Theta, \boldsymbol{C}_A, \boldsymbol{M}_i) \tag{16}$$

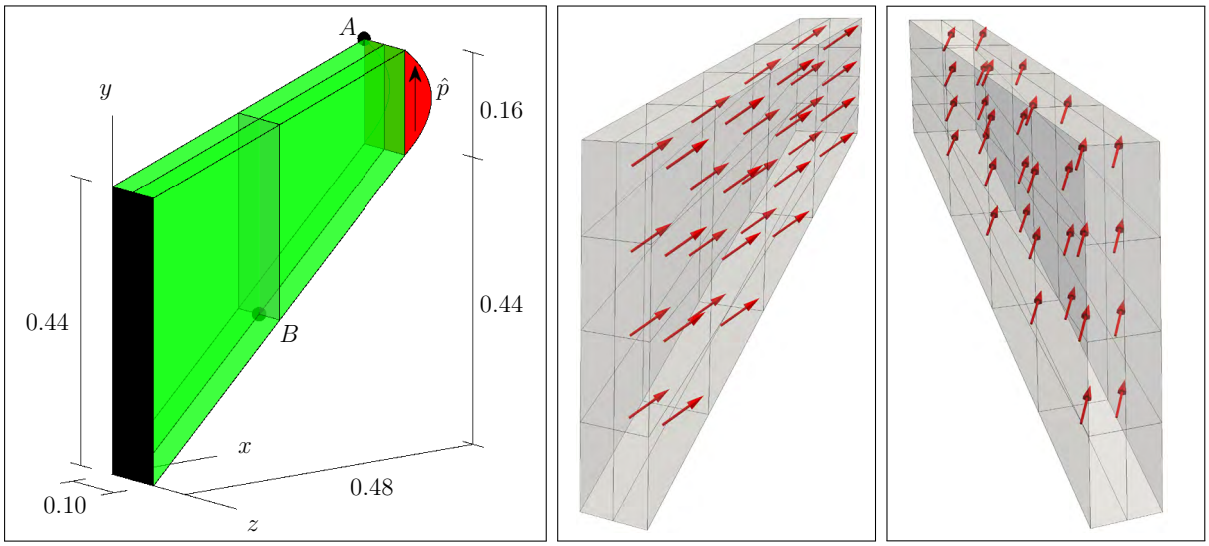

Figure 1: Geometry, configuration and fiber direction $(\mathbf{a}_0^1)^T = [1\ 1\ 1]$ of cooks cantilever beam.

At last we add the additional fields $\boldsymbol{H}_A$ and $\tilde{J}_A$ and the corresponding Lagrange multipliers $\boldsymbol{B}_A$ and $\tilde{p}_A$ we get the CoCoA element as shown in Reference [5]

$$\Pi_{HW}^{CoCoA}(\boldsymbol{q},\dots) = \Pi_{HW}^{CoSKA} + \int_{\mathcal{B}_0} \boldsymbol{B}_A : (\mathrm{cof}[\boldsymbol{C}] - \boldsymbol{H}_A)\mathrm{d}V + \int_{\mathcal{B}_0} \tilde{p}_A(J - \tilde{J}_A)\mathrm{d}V \quad \text{with} \tag{17}$$

$$\Psi_M(\dots) = \Psi_M^{iso}(\boldsymbol{C},\boldsymbol{H},\tilde{J}) + \Psi_M^{vol}(\tilde{J}) + \Psi_M^{cap}(\Theta) + \Psi_M^{coup}(\Theta,\tilde{J}) \tag{18}$$

$$\Psi_{F_i}(\dots) = \Psi_{F_i}^{ela}(\boldsymbol{C}_A,\boldsymbol{H}_A,\tilde{J}_A,\boldsymbol{M}_i) + \Psi_{F_i}^{cap}(\Theta) + \Psi_{F_i}^{coup}(\Theta,\boldsymbol{C}_A,\boldsymbol{M}_i) \tag{19}$$

Now, we apply the mixed principle of virtual power in Reference [7]. In this way, we can extend this formulation to dynamic problems. The basis is the total energy balance

$$\dot{T}(\dot{\boldsymbol{q}},\dot{\boldsymbol{v}},\dot{\boldsymbol{p}}) + \dot{\Pi}^{\mathrm{ext}}(\dot{\boldsymbol{q}},\boldsymbol{\lambda},\tilde{\Theta}) + \dot{\Pi}^{\mathrm{int}}(\dot{\boldsymbol{q}},\dot{\Theta},\dot{\eta},\tilde{\Theta},\boldsymbol{S}_A,\dot{\boldsymbol{C}}_A,\tilde{p},\dot{\tilde{J}},\boldsymbol{B},\dot{\boldsymbol{H}},\tilde{p}_A,\dot{J}_A,\boldsymbol{B}_A,\dot{\boldsymbol{H}}_A) = 0 \tag{20}$$

where the time derivative of the kinetic energy

$$\dot{T}(\dot{\boldsymbol{q}},\dot{\boldsymbol{v}},\dot{\boldsymbol{p}}) = \int_{\mathcal{B}_0} (\rho_0\boldsymbol{v} - \boldsymbol{p})\cdot\dot{\boldsymbol{v}}\mathrm{d}V + \int_{\mathcal{B}_0} \dot{\boldsymbol{p}}\cdot(\dot{\boldsymbol{q}} - \boldsymbol{v})\mathrm{d}V + \int_{\mathcal{B}_0} \boldsymbol{p}\cdot\ddot{\boldsymbol{q}}\mathrm{d}V \tag{21}$$

is defined by the velocity $\boldsymbol{v}$, the linear momentum $\boldsymbol{p}$ and the mass density ρ_0. As external power functional, we assume

$$\dot{\Pi}^{\mathrm{ext}}(\dot{\boldsymbol{q}},\boldsymbol{\lambda},\tilde{\Theta}) = -\int_{\partial\mathcal{B}_0} \boldsymbol{t}\cdot\dot{\boldsymbol{q}}\mathrm{d}A - \int_{\partial\mathcal{B}_0} \boldsymbol{\lambda}\cdot(\dot{\boldsymbol{q}} - \dot{\boldsymbol{q}}^{\mathrm{ref}})\mathrm{d}A + \int_{\mathcal{B}_0} \frac{1}{\Theta}\nabla\tilde{\Theta}\cdot\boldsymbol{Q}\mathrm{d}V. \tag{22}$$

Here, Dirichlet boundary conditions are modelled by Lagrange multipliers $\boldsymbol{\lambda}$. $\dot{\boldsymbol{q}}^{\mathrm{ref}}$ denotes the time evolution of Dirichlet boundary displacement vector, $\boldsymbol{t}$ denotes the traction load

for the Neumann boundary conditions and

$$\boldsymbol{Q} = -\left[\sum_{i=1}^{n_F} J\frac{k_{F_i} - k_M}{\boldsymbol{C} : \boldsymbol{M}_i}\boldsymbol{M}_i + kJ\boldsymbol{C}^{-1}\right]\nabla\Theta \tag{23}$$

denotes the Piola heat flux vector derived from Duhamel's law (see Reference [7]). Here k_m and k_{F_i} denotes the material conductivity coefficients for matrix and fibers. By variation with respect to the variables in the argument from Eqn. 20 (as shown in Reference [7]), we get the following weak forms of the CoCoA element:

$$\int_T\int_{\mathcal{B}_0}[\mathrm{Div}[\boldsymbol{F}\boldsymbol{S}] - \dot{\boldsymbol{p}}]\cdot\delta\dot{\boldsymbol{q}}\mathrm{d}V\mathrm{d}t = 0 \qquad \int_T\int_{\mathcal{B}_0}\left[\frac{1}{\rho_0}\boldsymbol{p} - \dot{\boldsymbol{q}}\right]\cdot\delta\dot{\boldsymbol{v}}\mathrm{d}V\mathrm{d}t = 0$$

$$\int_T\int_{\partial\mathcal{B}_0}[-\boldsymbol{t} - \boldsymbol{\lambda}]\cdot\delta\dot{\boldsymbol{q}}\mathrm{d}A\mathrm{d}t = 0 \qquad \int_T\int_{\partial\mathcal{B}_0}\left[\dot{\tilde{\boldsymbol{q}}} - \dot{\boldsymbol{q}}^{\mathrm{ref}}(t)\right]\cdot\delta\boldsymbol{\lambda}\mathrm{d}A\mathrm{d}t = 0$$

$$\int_T\int_{\mathcal{B}_0}\left[\Theta - \tilde{\Theta}\right]\delta\dot{\eta}\mathrm{d}V\mathrm{d}t = 0 \qquad \int_T\int_{\mathcal{B}_0}\left[\eta + \frac{\partial\Psi}{\partial\Theta}\right]\delta\dot{\Theta}\mathrm{d}V\mathrm{d}t = 0$$

$$\int_T\int_{\mathcal{B}_0}\left[\frac{\mathrm{Div}[\boldsymbol{Q}]}{\Theta} + \dot{\eta}\right]\delta\tilde{\Theta}\mathrm{d}V\mathrm{d}t = 0$$

$$\int_T\int_{\mathcal{B}_0}\frac{1}{2}\left[\dot{\boldsymbol{C}}_A - \dot{\boldsymbol{C}}\right] : \delta\boldsymbol{S}_A\mathrm{d}V\mathrm{d}t = 0 \qquad \int_T\int_{\mathcal{B}_0}\left[\frac{1}{2}\boldsymbol{S}_A - \frac{\partial\Psi}{\partial\boldsymbol{C}_A}\right] : \delta\dot{\boldsymbol{C}}_A\mathrm{d}V\mathrm{d}t = 0$$

$$\int_T\int_{\mathcal{B}_0}\left[\dot{\tilde{J}} - \dot{J}\right]\delta\tilde{p}\mathrm{d}V\mathrm{d}t = 0 \qquad \int_T\int_{\mathcal{B}_0}\left[\tilde{p} - \frac{\partial\Psi}{\partial\tilde{J}}\right]\delta\dot{\tilde{J}}\mathrm{d}V\mathrm{d}t = 0$$

$$\int_T\int_{\mathcal{B}_0}\left[\dot{\boldsymbol{H}} - \dot{\mathrm{cof}}[\boldsymbol{C}]\right] : \delta\boldsymbol{B}\mathrm{d}V\mathrm{d}t = 0 \qquad \int_T\int_{\mathcal{B}_0}\left[\boldsymbol{B} - \frac{\partial\Psi}{\partial\boldsymbol{H}}\right] : \delta\dot{\boldsymbol{H}}\mathrm{d}V\mathrm{d}t = 0$$

$$\int_T\int_{\mathcal{B}_0}\left[\dot{J}_A - \dot{J}\right]\delta\tilde{p}_A\mathrm{d}V\mathrm{d}t = 0 = 0 \qquad \int_T\int_{\mathcal{B}_0}\left[\tilde{p}_A - \frac{\partial\Psi}{\partial\tilde{J}_A}\right]\delta\dot{J}_A\mathrm{d}V\mathrm{d}t = 0$$

$$\int_T\int_{\mathcal{B}_0}\left[\dot{\boldsymbol{H}}_A - \dot{\mathrm{cof}}[\boldsymbol{C}]\right] : \delta\boldsymbol{B}_A\mathrm{d}V\mathrm{d}t = 0 \qquad \int_T\int_{\mathcal{B}_0}\left[\boldsymbol{B}_A - \frac{\partial\Psi}{\partial\boldsymbol{H}_A}\right] : \delta\dot{\boldsymbol{H}}_A\mathrm{d}V\mathrm{d}t = 0$$

As second Piola-Kirchhoff stress tensor, we obtain

$$\boldsymbol{S} = 2\frac{\partial\Psi}{\partial\boldsymbol{C}} + 2\boldsymbol{B} : \frac{\partial\mathrm{cof}[\boldsymbol{C}]}{\partial\boldsymbol{C}} + \tilde{p}J^{-1}\mathrm{cof}[\boldsymbol{C}] + \boldsymbol{S}_A + 2\boldsymbol{B}_A : \frac{\partial\mathrm{cof}[\boldsymbol{C}]}{\partial\boldsymbol{C}} + \tilde{p}_A J^{-1}\mathrm{cof}[\boldsymbol{C}]. \tag{24}$$

All quantities are approximated with Lagrangian shape functions in space (see Reference [4, 7]) and time (see Reference [7]). All exsisting integrals are solved with the corresponding Gaussian quadrature rule. We eliminate $\boldsymbol{p}$ and η and condense out the resulting formulation at the element level to a displacement and temperature formulation (see Reference [2]). Therefore, all mixed fields except $\boldsymbol{q}$ and Θ are discontinuous at the boundaries of spatial elements.

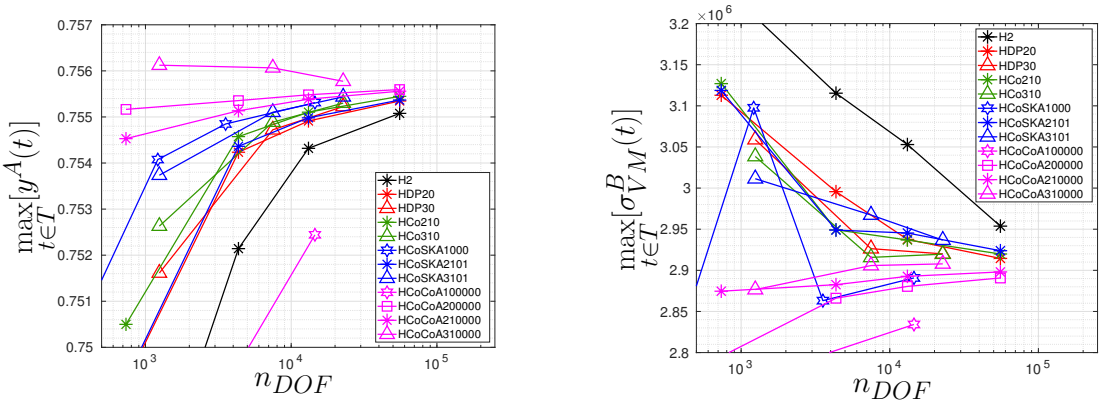

Figure 2: Convergence of the y-coordinate on point A and the v. Mises equivalence stress σ_{VM} on point B for the parameters shown in Table 1 and fiber F_1.

4 NUMERICAL EXAMPLES

As numerical example serves the well-known Cook's cantilever beam with a quadratic distribution of an in-plane load on the Neumann boundary. Two different fibers are used for this example. On the one side a fiber (F_1,$(\mathbf{a}_0^1)^T = [1\ 1\ 1]$) for mechanical reinforcement of the matrix, but with an equally low thermal conductivity. On the other side, a fiber (F_2,$(\mathbf{a}_0^1)^T = [1\ 1\ 0]$) with a very high thermal conductivity, but a low stiffness. The energy functions are given by

$$\Psi_M^{iso} = \frac{\epsilon_1}{2}(\mathrm{tr}[\boldsymbol{C}])^2 + \frac{\epsilon_2}{2}(\mathrm{tr}[\mathrm{cof}[\boldsymbol{C}]])^2 - \epsilon_3 \ln(J) \quad \Psi_M^{vol} = \frac{\epsilon_4}{2}(J^{\epsilon_5} + J^{-\epsilon_5} - 2)$$

$$\Psi_{F_1}^{ela} = \epsilon_6 \left(\frac{1}{\epsilon_7 + 1}(\mathrm{tr}[\boldsymbol{C}\boldsymbol{M}_1])^{\epsilon_7+1} + \frac{1}{\epsilon_8 + 1}(\mathrm{tr}[\mathrm{cof}[\boldsymbol{C}]\boldsymbol{M}_1])^{\epsilon_8+1} + \frac{1}{\epsilon_9}\det[\boldsymbol{C}]^{-\epsilon_9} \right)$$

$$\Psi_{F_2}^{ela} = \frac{\epsilon_{10}}{2}(\mathrm{tr}[\boldsymbol{C}\boldsymbol{M}_2] - 1)^2$$

$$\Psi_X^{cap} = c_X^0(1 - \Theta_\infty c_X^1)(\Theta - \Theta_\infty - \Theta \ln \frac{\Theta}{\Theta_\infty}) - \frac{1}{2}c_X^0 c_X^1(\Theta - \Theta_\infty)^2$$

and the prescribed simulation parameters, shown in Tab. 1. Geometry, configuration and fiber direction $(\mathbf{a}_0^1)^T = [1\ 1\ 1]$ of cooks cantilever beam are shown in Fig. 1. We compare the mixed finite elements up to cubic order and analyze the spatial convergence for some combinations of polynomial degrees in space of the independent quantities and the effect on the thermo-mechanical coupling. In the second step, we analyze the option of directional heat conduction using the fibers. The element title starts with H for hexahedral element and is followed by the element type and the information about the polynomial degrees of all quantities (see Table 2). Fig. 2 shows the convergence of the y-coordinate and the stress σ_{VM} of some elements. These element selection is based on the results from Reference [5] and is a selection of the best elements of each element type. They show the same behavior for the spatial convergence. CoCoA elements with a low polynomial degree for the quantities of the anisotropic part have the highest convergence rate, followed by the

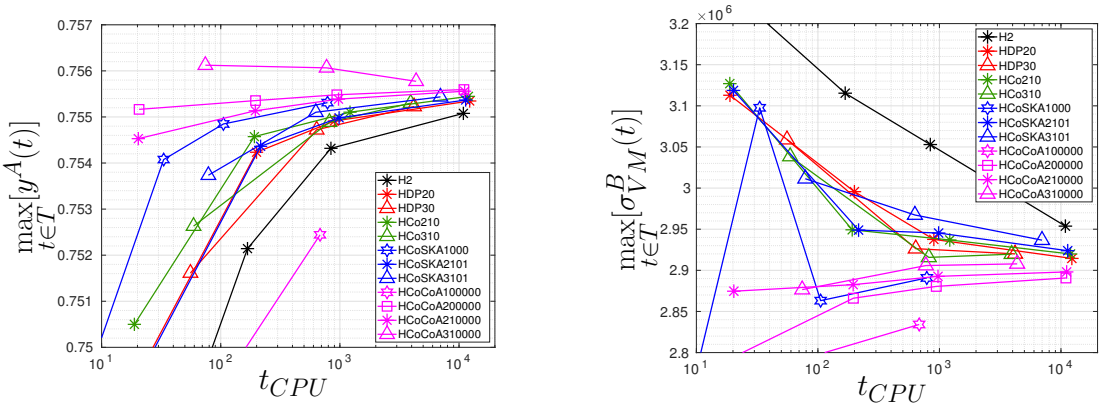

Figure 3: Convergence of the y-coordinate on point A and the v. Mises equivalence stress σ_{VM} on point B for the parameters shown in Table 1 and fiber F_1.

CoFEM elements and the standard elements. Also, the HCoSKA1000 element represents a special case and has a very high convergence rate of the y-coordinate for a linear element. Nevertheless, you can see a strong oscillation in the convergence rate of σ_{VM}.

This also has a direct effect on the computing time. Fig. 3 shows the same curves over the computational time. The high convergence rate saves at least one order of magnitude in computational time, because coarse meshes are sufficient for accurate solutions in space. This plays all the more a role for thermo-mechanical systems, since here not only the degrees of freedom increase by a third, also the symmetry of the tangents matrix is lost.

Furthermore, Figs. 4, 5 and 6 show the deformed elements together with the v. Mises equivalence stress σ_{VM} at different discretization levels. Here you can also see, that the CoCoA and SKA elements show a very good convergence and with $n_{el} = 256$ they provide nearly the same solution as with $n_{el} = 4000$. All elements show the asymmetric bending caused by the fiber as well as the typical stress curve (tensile and compressive stress, neutral fiber). Fig. 7 shows that the different solutions in the displacement have a corresponding effect on the thermo-mechanical coupling. While no temperature change can be seen in the standard elements, it is clearly visible for the mixed elements (especially on the Dirichlet boundary). However, it is not possible to say which solution is the optimal one, further tests have to be performed.

In the next step, we add the second fiber (F_2) and a linear start temperature distribution as shown in Fig. 9. Because of the high conductivity of the second fiber, the temperature in cook's cantilever beam is distributed much faster (see Fig. 10).

At least we check the conservation properties on the example of the HSCoCoA210000 element with two fibers (see Fig. 8). For instance, the angular momentum ($\boldsymbol{L}$) is preserved, as the theory for Galerkin-based time integrators with Gaussian quadrature predicts. But, over the entire simulation period, we get a significant error in the energy (E). This was to be expected, because we do not use an energy momentum scheme to preserve the energy balance.

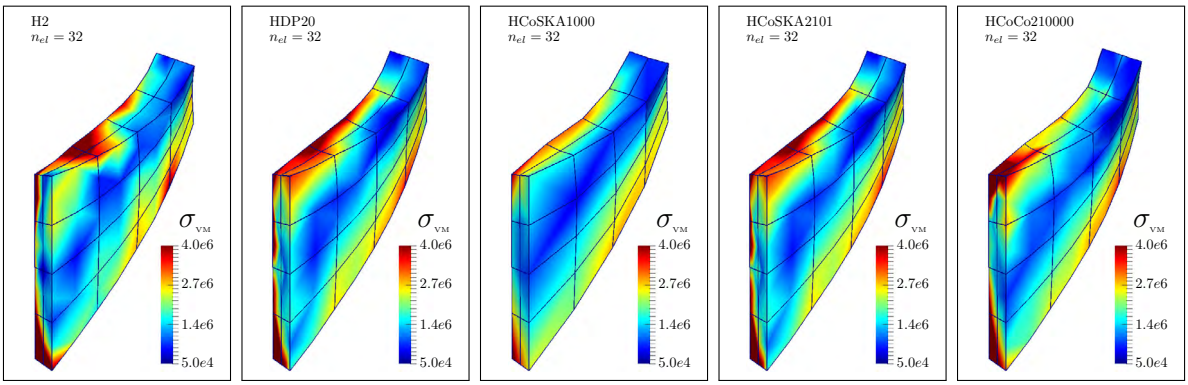

Figure 4: Deformed configuration $\mathcal{B}_t$ and v. Mises equivalent stress σ_{VM} for the parameters shown in Table 1 and fiber F_1 for $t = 1$. Cook's cantilever beam with $n_{el} = 32$ spatial finite elements.

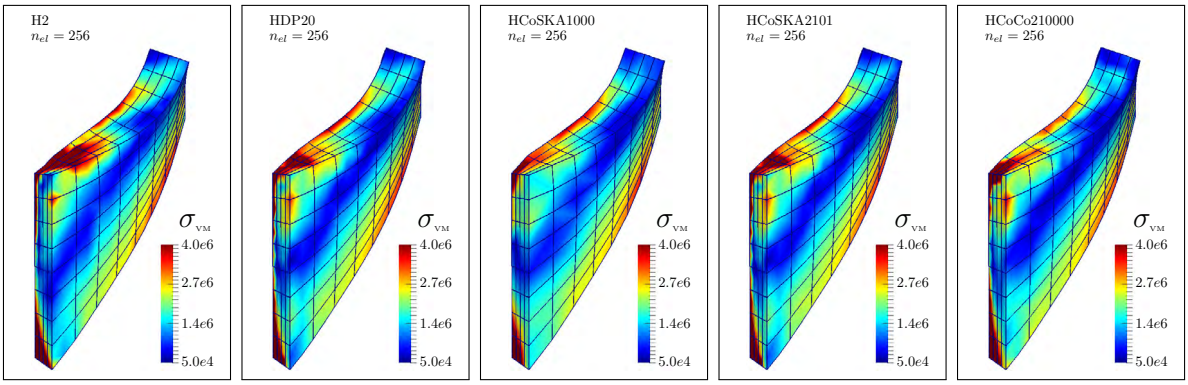

Figure 5: Deformed configuration $\mathcal{B}_t$ and v. Mises equivalent stress σ_{VM} for the parameters shown in Table 1 and fiber F_1 for $t = 1$. Cook's cantilever beam with $n_{el} = 256$ spatial finite elements.

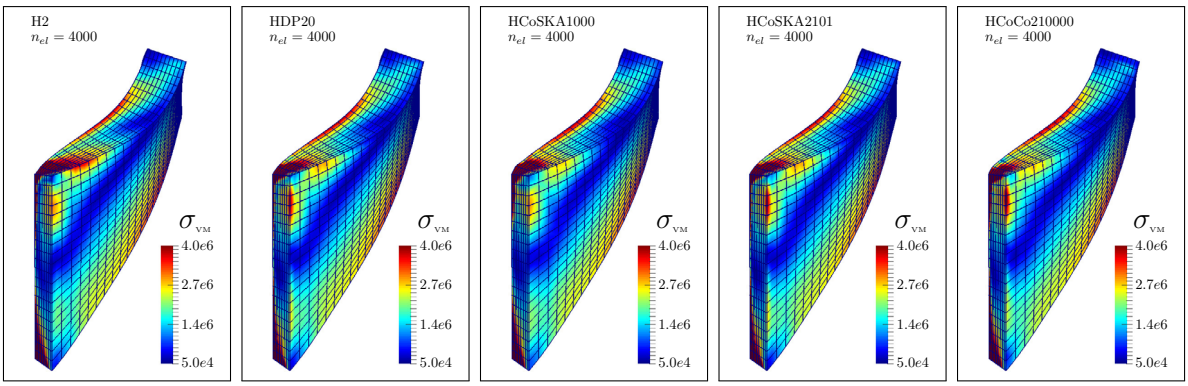

Figure 6: Deformed configuration $\mathcal{B}_t$ and v. Mises equivalent stress σ_{VM} for the parameters shown in Table 1 and fiber F_1 for $t = 1$. Cook's cantilever beam with $n_{el} = 4000$ spatial finite elements.

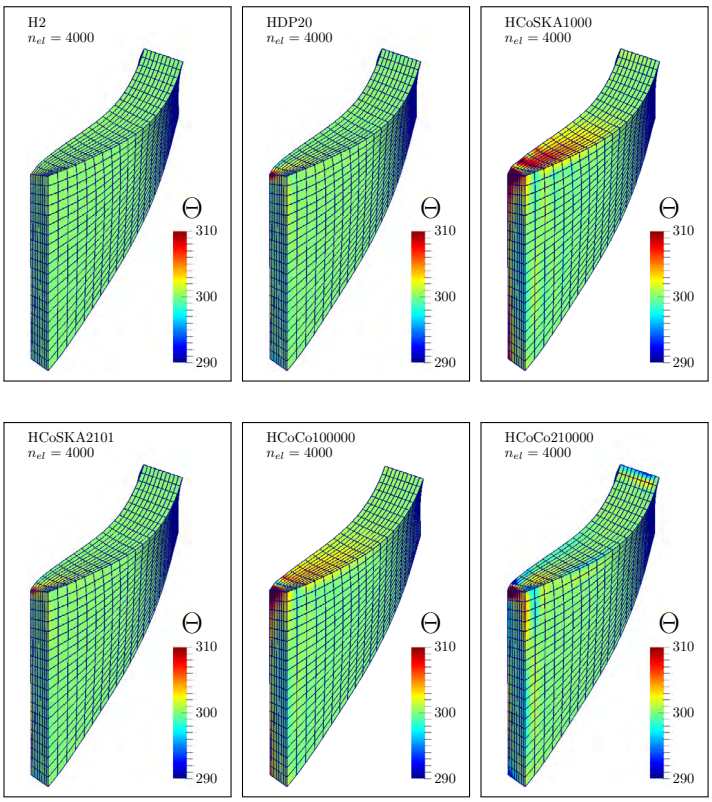

Figure 7: Deformed configuration $\mathcal{B}_t$ and temperature Θ for the parameters shown in Table 1 and fiber F_1 for $t = 1$. Cook's cantilever beam with $n_{el} = 4000$ spatial finite elements.

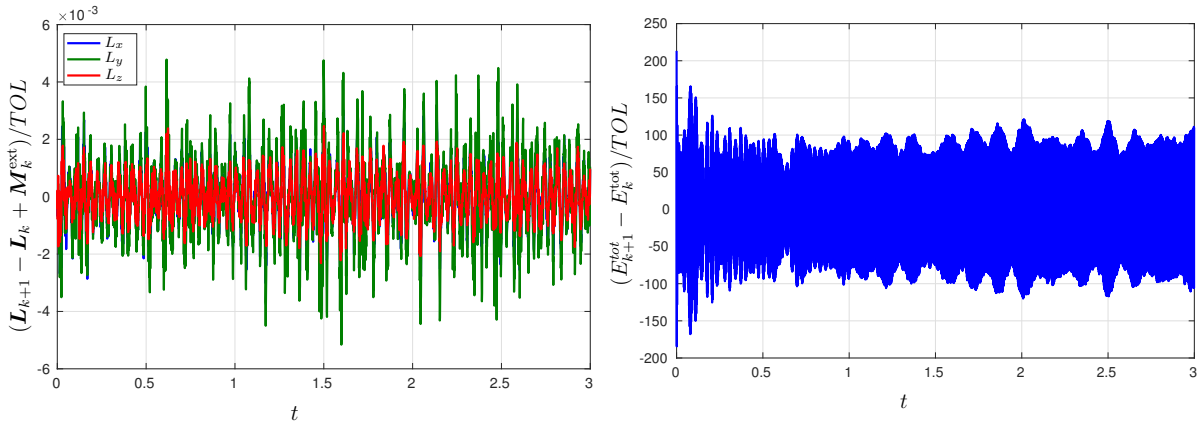

Figure 8: Conservation properties of the HSCoCoA210000 element for the parameters shown in Table 1 for $n_{el} = 256$ and fibers F_1 and F_2.

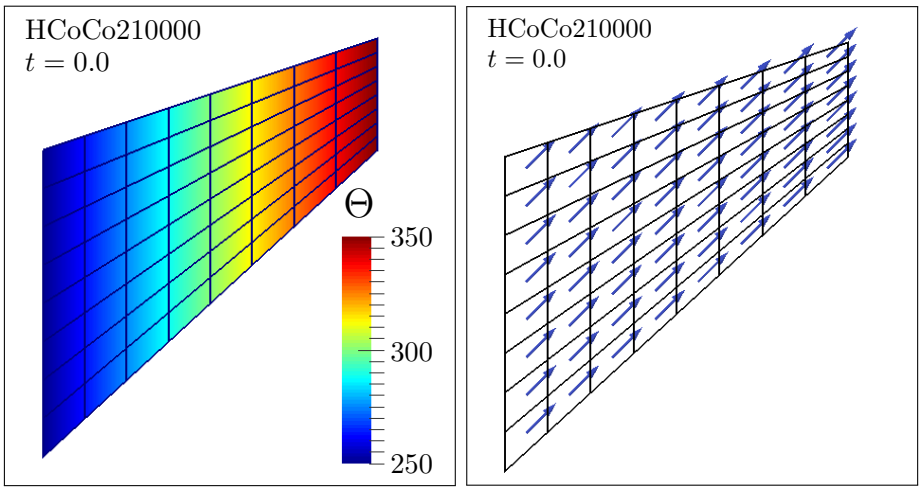

Figure 9: Temperature distribution and fiber direction $(\mathbf{a}_0^2)^T = [1\ 1\ 0]$ of cooks cantilever beam.

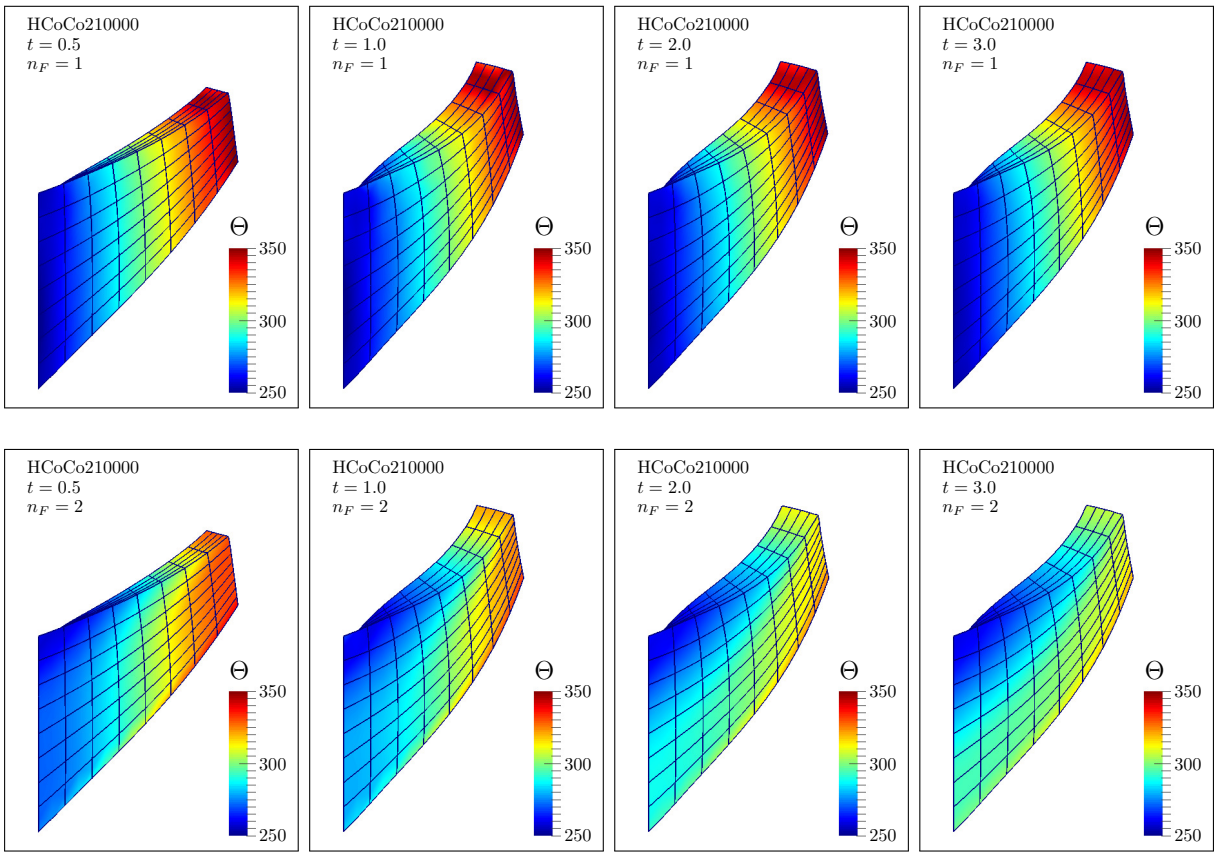

Figure 10: Deformed configuration $\mathcal{B}_t$ and temperature Θ for the parameters shown in Figure 1 for $n_{el} = 256$ and fibers F_1 and F_2 of Cook's cantilever beam.

5 CONCLUSIONS

We were able to show that the excellent performance of the mixed elements is still preserved in a thermo-mechanical context. This especially has very good effects on the computing time. Furthermore we have the possibility to determine the mechanical and thermal properties of our model separately by using different fibers. In the next step, we extend this formulation to an energy conserving time integrator and implement thermal Dirichlet and Neumann boundary conditions.

ACKNOWLEDGEMENTS

The authors thank the 'Deutsche Forschungsgesellschaft (DFG)' for financial support of this work under the grant GR 3297/4-1 and Matthias Bartelt (GR 3297/2-2) for providing the program code and help with its implementation.

REFERENCES

[1] Simo, J., Taylor, R., Pister., K., 1985. Variational and projection methods for the volume constraint in finite deformation elasto-plasticity. Computer Methods in Applied Mechanics and Engineering 1:177—208.

[2] Schröder, J., Wriggers, P., Balzani, D. (2011) A new mixed finite element based on different approximations of the minors of deformation tensors. *Comput. Methods Appl. Mech. Engrg.*, 49:3583–3600.

[3] Schröder, J., Viebahn, V., Wriggers, P., Balzani, D. (2016) A novel mixed finite element for finite anisotropic elasticity; the SKA-element Simplified Kinematics for Anisotropy. *Comput. Methods Appl. Mech. Engrg.*, 310:475–494.

[4] Bartelt, M., Dietzsch., J., Groß., M., 2018. Efficient implementation of energy conservation for higher order finite elements with variational integrators. Mathematics and Computers in Simulation, in press, DOI 10.1016/j.matcom.2018.03.0.

[5] Dietzsch J. and Groß M. (2018), MIXED FINITE ELEMENT FORMULATIONS FOR THE GALERKIN-BASED TIME INTEGRATION OF FINITE ANISOTROPIC ELASTODYNAMICS. *ECCOMAS conference ECCM-ECFD 2018* - 6th European Conference on Computational Mechanics (ECCM 6), Glasgow UK, 11-15 June 2018

[6] Groß, M., Dietzsch., J. (2017) Variational-based energy–momentum schemes of higher-order for elastic fiber-reinforced continua. *Comput. Methods Appl. Mech. Engrg.*, 320:509–542.

[7] Groß M., Dietzsch J. and Bartelt M. (2018), Variational-based higher-order accurate energy–momentum schemes for thermo-viscoelastic fiber-reinforced continua, *Comput. Methods Appl. Mech. Engrg.*, 336: 353-418, 2018.